

ECF22 - Loading and Environmental effects on Structural Integrity

Validating 3D two-parameter fracture mechanics for structural integrity assessments

C.A. Simpson^{a*}, S. Tonge^a, A. Cinar^a, C. Reinhard^b, T.J. Marrow^c, M. Mostafavi^a^a Department of Mechanical Engineering, University of Bristol, University Walk, Bristol, BS8 1TR, UK^a DIAD Beamline, Diamond Light Source, Harwell Science & Innovation Campus, Didcot OX11 0DE, UK^c Department of Materials, University of Oxford, Oxford OX1 3PH, UK

Abstract

In-situ fracture tests were carried out on the I12 beamline at the Diamond Light Source. Four Al-Ti metal-matrix composites (MMCs), with varying combinations of thickness and crack length, were studied to assess for the impact of in-plane and out-of-plane constraint. Synchrotron X-ray computed tomography and synchrotron X-ray diffraction were used to measure total strain and elastic strain respectively. The total strain was calculated via digital volume correlation, with Ti particles within the MMC providing sufficient texture to track the internal displacement vectors in 3D. The total, elastic-plastic strain energy release rate, J_{total} was calculated from 2D slices extracted from the 3D displacement field, with J_{total} reaching a maximum value at the sample surface. It is, however, still unclear whether calculating J_{total} on a slice-by-slice basis provides an accurate representation of strain energy release rate across the crack front; techniques to evaluate the J-integral from the full 3D displacement field are being developed.

© 2018 The Authors. Published by Elsevier B.V.

Peer-review under responsibility of the ECF22 organizers.

Keywords: strain energy release rate; J-integral; plastic constraint; XRD; XCT; DVC; DIC

1. Introduction

Understanding the impact of constraint on fracture behaviour is central to the accurate, non-conservative life assessment of safety critical structural components used in the aerospace and nuclear industries. The fracture resistance of cracked bodies with low levels of plastic constraint is significantly under-estimated when using a single parameter

* Corresponding author.

E-mail address: c.simpson@bristol.ac.uk

fracture assessment. Attempts are therefore made to account for the impact of constraint in integrity assessment standards such as R5 using fracture parameters such as T , Q and T_z (Mu, Wang, Tu, & Xuan, 2016). These parameters are, however, only sensitive to either in-plane (T , Q) or out-of-plane (T_z) constraint. There is therefore a need to improve on the current methodology and move towards a simple, unified parameter that better addresses both in-plane and out-of-plane constraint. Recently there have been promising advances, with authors such as Mostafavi et al. (2010) and Yang et al. (2013) detailing parameters that attempt to capture the extent or volume of plasticity around the crack tip as a function of constraint. While these parameters have been shown to be sensitive to both in-plane and out-of-plane constraint, there is still more fundamental research required to properly quantify and validate the dependence of fracture toughness on 3D plastic constraint (i.e. loss of both in-plane and out of plane constraint). To that end, we use a novel combination of synchrotron X-ray diffraction (XRD) and X-ray computed tomography (XCT) to study and separate the elastic and plastic contributions to strain energy release rate with respect to both 3D plastic constraint and through thickness position. The following work details the methodology used and some of the initial results.

2. Methodology

2.1. Material and Samples

Fracture tests were carried out, in-situ, at the Diamond Light Source on the I12:JEEP beamline (Drakopoulos et al., 2015), on Al-Ti metal matrix composite (MMC) double edge notch tension (DENT) samples. These samples had varying sample thicknesses (b) and crack lengths (a); this test matrix was chosen to allow for the assessment of varying levels of 3D plastic constraint on fracture and is detailed in Table 1. This research is still ongoing and the initial results for the two thinner specimens ($b = 5$ mm) are presented here alongside the novel measurement methodology and analysis approach. The experimental setup and sample geometry can be seen in Figure 1.

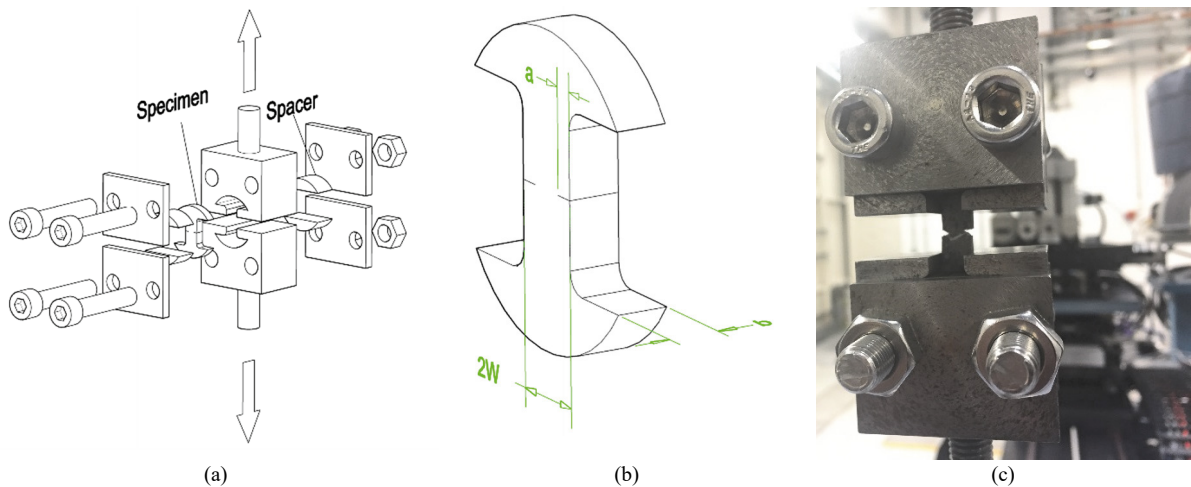


Fig. 1. Overview of the experiment setup. (a) Schematic view of the loading details; (b) DENT specimen where a is the crack length, W the width and b its thickness; (c) a fractured specimen inside the loading jig at EH2

Testing was carried out on a 10 kN Shimadzu loading frame, which was mounted in Experimental Hutch 2 (EH2), which was designed to accommodate large experimental setups. The fracture behaviour was interrogated through a combination of (a) XRD and (b) XCT or, more specifically, through the associated use of digital volume correlation (DVC). XRD allows for measurement of through thickness averaged elastic strain, while DVC allows for the characterisation of the total 3D displacement or strain field as a function of position through thickness. While the measurements could not be made simultaneously, the acquisition mode could be switched semi-automatically in under 10 minutes, allowing elastic and total strain measurements to be made under effectively identical conditions. XRD and XCT were carried out at 7 load increments between 50 N and fracture, which occurred at 4.5 kN and 4.0 kN at $a/W = 0.1$ and $a/W = 0.5$ respectively.

Table 1. Test matrix for the full program of work, highlighting the in-plane and out-of-plane constraint with respect to sample geometry and crack length. The tests highlighted in green are the subject of the current paper.

	b = 5 mm	b = 20 mm
a/W = 0.1	Low in-plane Low out-of-plane	Low in-plane High out-of-plane
a/W = 0.5	High in-plane Low out-of-plane	High in-plane High out-of-plane

2.2. Synchrotron X-ray Diffraction

Monochromatic XRD was used to measure the elastic strain distribution in the Al-Ti MMC samples using a 2D Thales Pixium RF4343 area detector (2881 x 2880 pixels) and a beam energy of 60 keV. The sample to detector distance of 1.5 m allowed for a maximum diffracted angle, $2\theta = 8^\circ$ and the acquisition of seven Al peaks and four Ti peaks. Diffraction patterns were acquired using an incoming slit size of 0.1 mm square. The initial pre-processing of the data leveraged the DAWN analysis suite (Filik et al., 2017), with the Debye-Scherrer rings being azimuthally integrated across 5° windows. At each loading stage and for both the sample at (a) $a/W = 0.1$ and (b) $a/W = 0.5$, diffraction data was acquired across a 2D grid. Each map consisted of approximately 500 points across an area 8 mm x 4 mm with a point spacing of 0.3 mm. In the area surrounding the notch tip, the point density was higher, with an associated spatial resolution of 0.15 mm. The increase in spatial resolution was chosen to better capture the high strain gradient observed in this region. An example of the integrated diffraction pattern can be seen in Figure 2.

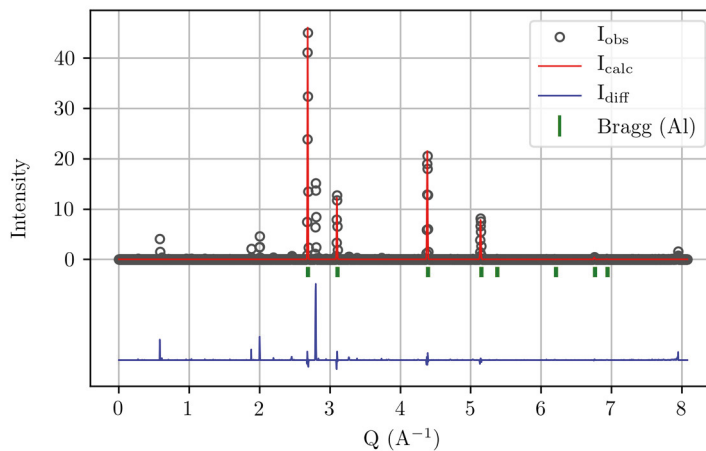


Fig. 2. Diffraction pattern acquired from the Al-Ti MMC. The red line which overlays the integrated diffraction data highlights a Pawley refinement on the Al peaks. The unfitted peaks correspond to reflections from the Ti particles.

2.3. Limited Angle X-ray Computed Tomography

The loading rig restricted the angles over which radiographs could be acquired and, as such, limited angle computed tomography was performed over an angular range of 145° at a beam energy of 60 keV. 2501 projections were acquired using an exposure time of 0.05 s, with the 3D tomograms then being reconstructed using a filtered back-projection algorithm. The difference in attenuation coefficient between the low-density Al-matrix and higher density Ti particles allows the Ti particles to be distinguished from the matrix (see Figure 4a). These particles provide texture and act in a manner analogous to the speckle pattern in 2D digital image correlation, allowing local displacement vectors to be tracked in a 3D solid. The digital volume correlation was performed relative to tomograms acquired on the undeformed, nominally unloaded sample (50 N). The analysis was completed using the DaVis 8.4 software from LaVision. DVC analysis of the tomograms was completed with a subset size of 16 voxels with 80% overlap.

3. Results and Discussion

3.1. Elastic strain fields

A multi-peak, Pawley refinement was used to evaluate the peak shifts and associated strain with respect to load in the Al matrix using the pyXe strain analysis package (Simpson, 2016). The Pawley refinement of the Al matrix is overlaid on the integrated diffraction profile shown in Figure 1, with the unfitted peaks corresponding to reflections associated with the Ti particles. Strain was calculated from peak shifts relative to a strain free, far field measure of the lattice parameter, a_0 (Withers, Preuss, Steuwer, & Pang, 2007) measured at minimum load such that $\varepsilon = (a - a_0) / a_0$. Further details of the diffraction analysis procedure can be found in the work of Mostafavi et al. (Mostafavi et al., 2017). Two examples of the 2D elastic strain field maps can be seen in Figure 3; these detail the elastic strain field at 4kN when a) $a/W = 0.1$ and b) $a/W = 0.5$. Line profiles were also extracted from these maps using 2D linear interpolation, with the lines being taken at the centre of the notch, where $y = 0$. The line profiles, shown as a function of applied load, can be seen in Figure 4. As noted, the strain maps and associated line profiles detail the strain in the Al matrix; as part of the broader study, efforts will be made to calculate the elastic strain from the Ti particles. This will allow the load partitioning between the two phases to be assessed. Work is also ongoing to determine the elastic component of the strain energy release rate, J_{elastic} from the 2D strain maps using JMAN_S (Barhli et al., 2016). JMAN_S uses Cholesky factorisation to calculate the displacement field from the in-plane strain tensors field. The displacement field (and the associated stress field) are then used to calculate J_{elastic} via a contour integral approach.

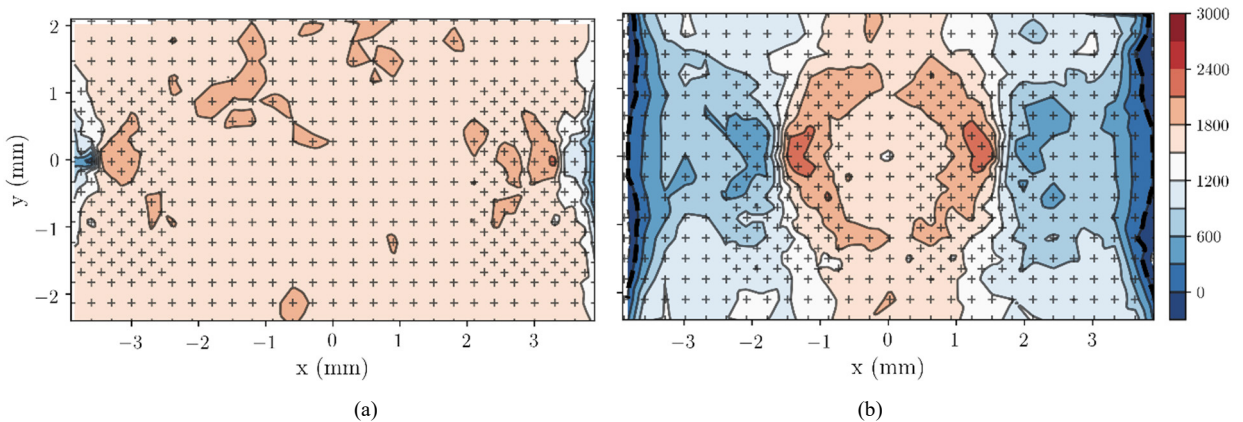


Fig. 3. 2D elastic strain (ε_{yy}) fields acquired using XRD at an applied load of 4 kN for (a) $a/W = 0.1$; (b) $a/W = 0.5$.

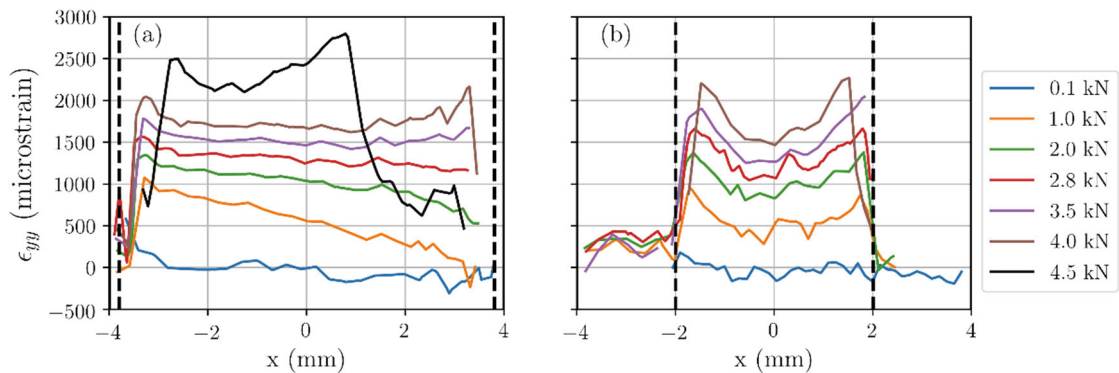


Fig. 4. Line profiles extracted from the 2D elastic strain maps as a function of load at (a) $a/W = 0.1$; (b) $a/W = 0.5$.

3.2. Displacement fields and total strain energy release rate

An example of a 2D slice through the 3D tomogram extracted at mid-thickness, acquired at a load of 4.5 kN for the sample with low in-plane constraint i.e. $a/W = 0.1$ can be seen in Figure 4a. Note the crack extension from the notch located on the right-hand side of the image, the effects of which can also be seen on the XRD profiles presented in Figure 43a. The associated displacement field, centred around one of the cracks, parallel to the loading axis and computed using DVC can be seen in Figure 5b.

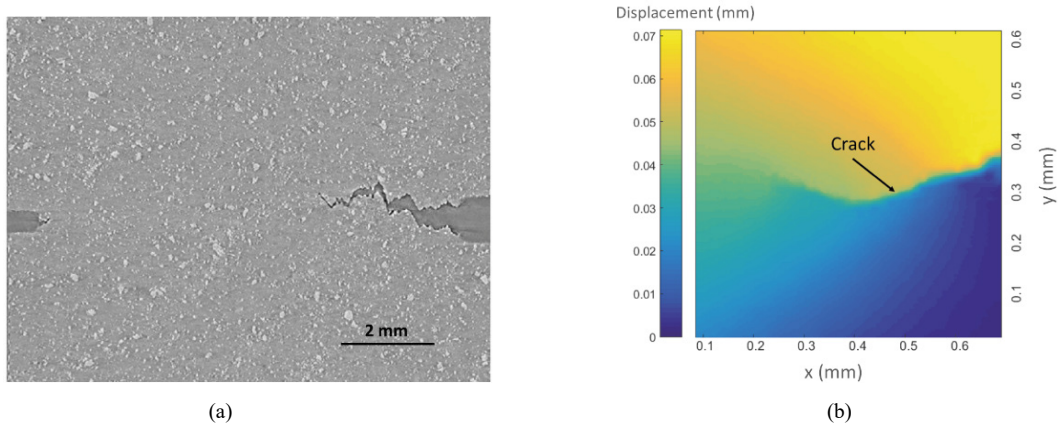


Fig. 5. (a) A reconstructed virtual slice extracted from a 3D tomogram; (b) displacement field (U_y) of a virtual slice calculated by DVC.

An in-house 3D phase congruency (PC) map code (Cinar et al., 2017), developed at the University of Bristol in collaboration with University of Oxford, was used to segment the crack highlighted in Figure 5b and calculate the 3D crack opening displacement profile (Figure 6a). The full-field elastic-plastic displacement field was then imported into ABAQUS using the OUR-OMA software tool (Barhli, Mostafavi, Cinar, Hollis, & Marrow, 2017), which optimizes the mesh and boundary conditions, introducing a free to deform region in the vicinity of the PC derived crack path. The total (elastic + plastic) strain energy release rate, J_{total} , was then automatically calculated via the domain integral method, which is built into ABAQUS. These values were converted into an equivalent stress intensity factor, K_I , where $K_I = \sqrt{J E}$. The variation in stress intensity factor as a function of position through the sample thickness can be seen in Figure 6b.

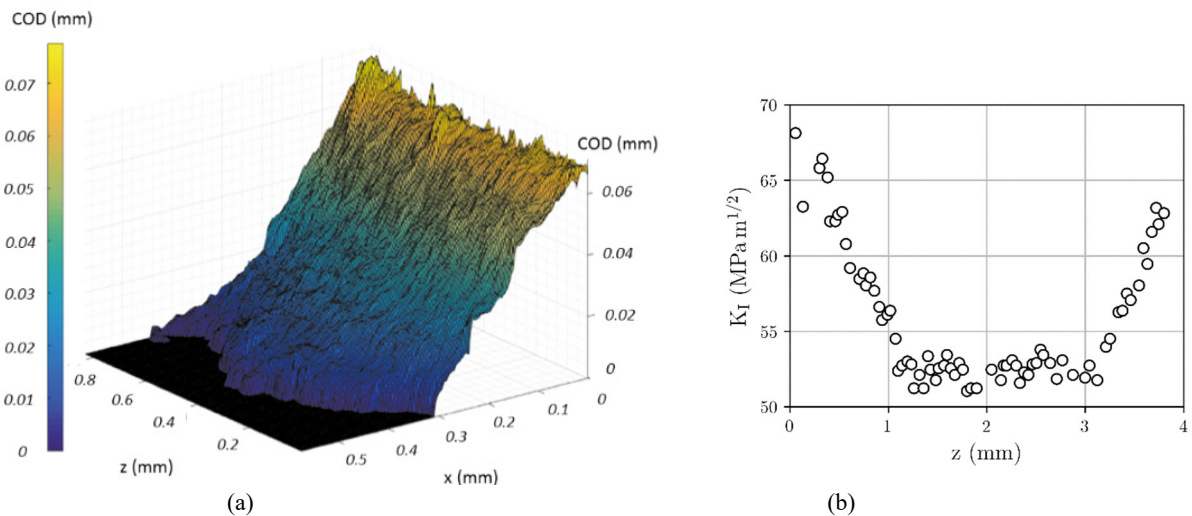


Fig. 6. (a) Three-dimensional map of crack opening displacement; (b) the variation in the stress intensity factor with respect to through thickness position for the sample tested at an a/W of 0.1.

Contrary to results previously published by Petit and Dodds (2004), the stress intensity factor appears to reach a minimum at the sample centre, tending towards a maximum value of almost 70 MPa m^{1/2} towards the free surface. It is still unclear whether this trend is valid as each slice is considered in isolation i.e. the OUR-OMA analysis is completed in a step-wise manner, iterating slice by slice across the 3D volume. To properly assess whether these findings are correct, further work is ongoing to convert the 2D OUR-OMA codebase into a 3D equivalent.

4. Conclusions

In this paper we have shown the initial results from a comprehensive experiment, which has leveraged developments in measuring elastic and elastic-plastic deformation fields using synchrotron X-ray diffraction and tomography pioneered by a long-term collaboration between Bristol and Oxford Universities. The through thickness variation total strain energy release rate has been calculated, and while there are some questions over its near surface validity, this is an important step towards an improved understanding of the impact of 3D plastic constraint on fracture. The corresponding through-thickness averaged elastic strains have been measured and will be fed into the JMAN_S analysis package, which will allow for the extraction of elastic strain energy release rate and ultimately the separation of the elastic and plastic contribution to strain energy release rate.

Acknowledgements

We thank Diamond Light Source for access to beamline I12 (EE12606-2) that contributed to the results presented here.

References

- Barhli, S. M., Mostafavi, M., Cinar, A. F., Hollis, D., & Marrow, T. J. (2017). J-Integral Calculation by Finite Element Processing of Measured Full-Field Surface Displacements. *Experimental Mechanics*, 57(6), 997–1009. <http://doi.org/10.1007/s11340-017-0275-1>
- Barhli, S. M., Saucedo-Mora, L., Simpson, C., Becker, T., Mostafavi, M., Withers, P. J., & Marrow, T. J. (2016). Obtaining the J-integral by diffraction-based crack-field strain mapping. *Procedia Structural Integrity*, 2, 2519–2526. <http://doi.org/10.1016/j.prostr.2016.06.315>
- Cinar, A. F., Barhli, S. M., Hollis, D., Flansbjerg, M., Tomlinson, R. A., Marrow, T. J., & Mostafavi, M. (2017). An autonomous surface discontinuity detection and quantification method by digital image correlation and phase congruency. *Optics and Lasers in Engineering*, 96, 94–106. <http://doi.org/10.1016/j.optlaseng.2017.04.010>
- Drakopoulos, M., Connolley, T., Reinhard, C., Atwood, R., Magdysyuk, O., Vo, N., ... Wanelik, K. (2015). I12: the Joint Engineering, Environment and Processing (JEEP) beamline at Diamond Light Source. *Journal of Synchrotron Radiation*, 22(3), 828–838. <http://doi.org/10.1107/S1600577515003513>
- Filik, J., Ashton, A. W., Chang, P. C. Y., Chater, P. A., Day, S. J., Drakopoulos, M., ... Wilhelm, H. (2017). Processing two-dimensional X-ray diffraction and small-angle scattering data in DAWN 2. *Journal of Applied Crystallography*, 50, 959–966. <http://doi.org/10.1107/S1600577517004708>
- Mostafavi, M., Collins, D. M., Peel, M. J., Reinhard, C., Barhli, S. M., Mills, R., ... Connolley, T. (2017). Dynamic contact strain measurement by time-resolved stroboscopic energy dispersive synchrotron X-ray diffraction. *Strain*, 53(2), 1–13. <http://doi.org/10.1111/str.12221>
- Mostafavi, M., Smith, D. J., & Pavier, M. J. (2010). Reduction of measured toughness due to out-of-plane constraint in ductile fracture of aluminium alloy specimens. *Fatigue and Fracture of Engineering Materials and Structures*, 33(11), 724–739. <http://doi.org/10.1111/j.1460-2695.2010.01483.x>
- Mu, M. Y., Wang, G. Z., Tu, S. T., & Xuan, F. Z. (2016). Three-dimensional analyses of in-plane and out-of-plane crack-tip constraint characterization for fracture specimens. *Fatigue and Fracture of Engineering Materials and Structures*, 39(12), 1461–1476. <http://doi.org/10.1111/ffe.12461>
- Petti, J. P., & Dodds, R. H. (2004). Coupling of the Weibull stress model and macroscale models to predict cleavage fracture. *Engineering Fracture Mechanics*, 71(13–14), 2079–2103. <http://doi.org/10.1016/j.engfracmech.2003.08.004>
- Simpson, C. A. (2016, April 21). pyxe: XRD Strain Analysis. <http://doi.org/10.5281/zenodo.50185>
- Withers, P. J., Preuss, M., Steuwer, A., & Pang, J. W. L. (2007). Methods for obtaining the strain-free lattice parameter when using diffraction to determine residual stress. *Journal of Applied Crystallography*, 40(5), 891–904. <http://doi.org/10.1107/S0021889807030269>
- Yang, J., Wang, G. Z., Xuan, F. Z., & Tu, S. T. (2013). Unified characterisation of in-plane and out-of-plane constraint based on crack-tip equivalent plastic strain. *Fatigue and Fracture of Engineering Materials and Structures*, 36(6), 504–514. <http://doi.org/10.1111/ffe.12019>